Quantum Molecular Dynamics Simulations Regarding the Dechlorination of Trichloro Ethene in the Interlayer Space of the 2:1 Clay Mineral Nontronite

Brian J. Teppen,[†] Ching-Hsing Yu,[‡] Susan Q. Newton,[‡] David M. Miller,[§] and Lothar Schäfer*[,‡]

Department of Crop and Soil Sciences, Michigan State University, East Lansing, Michigan 48824-1325, Department of Chemistry and Biochemistry, University of Arkansas, Fayetteville, Arkansas 72701, and Crop, Soil, and Environmental Sciences Department, University of Arkansas, Fayetteville, Arkansas 72701

Received: August 17, 2001; In Final Form: March 14, 2002

Quantum mechanical geometry optimizations and molecular dynamics simulations were performed of trichloroethene (TCE) adsorbed on the mineral surfaces in the interlayer space of an idealized nontronite, a 2:1 clay mineral containing structural Fe^{2+}. Density functional procedures were used as implemented in the ab initio program CASTEP, in fully periodic calculations. Geometry optimization included the atomic positions of the mineral and the adsorbates within the unit cell, in addition to unit cell lengths and angles, achieving full optimization of the entire crystal system. In the absence of water, TCE molecules reside flat on the mineral basal planes and the molecular structure is not significantly different from that of the isolated system. In the presence of water, geometry optimization leads to a nonplanar structure, with the *cis*-Cl−C═C−Cl torsion at 52.5° and a C···Cl distance of ∼3 Å. The molecular dynamics simulations show that the elongated C···Cl distance has lost the oscillatory properties of a true bond, which are clearly observed for the other bond distances of TCE, with frequencies of the right order of magnitude. The crystal lattice of the optimized nontronite with TCE and water in the interlayer space shows the structural features of oxidized nontronite, even though the starting structure was that of the reduced nontronite. The results make it promising to test the possibilities of joint computational and experimental techniques in finding the best conditions under which catalytic processes on clay mineral surfaces will occur.

Introduction

Nontronites are the expandable, dioctahedral clay minerals in which iron, rather than aluminum, populates the octahedral sheet. Nontronites serve as environmental redox catalysts in that their reduction does not cause mineral dissolution or radical structural change and is apparently fully reversible with respect to the oxidation state.[1−6] The catalytic properties of nontronites are relied upon for several schemes aimed to reductively dechlorinate organic contaminants in groundwater aquifers.[7−14] Knowledge of the mechanism by which nontronites mediate the reductive dechlorination of organic contaminants is desirable because it should allow engineers to optimize conditions that favor dechlorination reactions. In previous studies, it was found that different mechanisms apply to compounds which have different hydrolysis and redox potentials.[13,14]

For the current paper, we optimized the structure of trichloroethene (TCE) in the interlayer space of an idealized nontronite, using the quantum mechanical techniques of program CASTEP.[15] The study was prompted by our general interest in exploring the potential of computational techniques to provide information on chemical reactions on mineral surfaces. For TCE, specifically, we wanted to determine whether the interactions with the mineral surface would lead to distortions which can be thought to lower the activation energy of a dechlorination reaction. The results are reported below.

* To whom correspondence should be addressed.
[†] Michigan State University.
[‡] Department of Chemistry and Biochemistry, University of Arkansas.
[§] Crop, Soil, and Environmental Sciences Department, University of Arkansas.

Methods

As a starting point for the current study, we used the approximate structure for oxidized microcrystalline nontronite $Na(AlSi_7)Fe_4O_{20}(OH)_4$ that was recently obtained by Manceau et al.[16] The negative charge in the idealized clay lattice, balanced by Na^+, is 117 cmol/kg. We added structural protons (lacking in the X-ray structure) such that all Fe^{3+} occupy cis sites,[6] and we fully optimized the electronic structure, atomic positions, and unit cell vectors using the periodic ab initio program CASTEP.[15]

The ultimate goal of quantum mechanical calculations of minerals is to compute a wave function for the entire crystal. This can be done approximately through semiempirical means[17] and extended Hückel techniques.[18−20] The program CRYSTAL was developed[21−23] for computing more accurate HF/ab initio crystal wave functions, but applied to various minerals,[24−28] the computational demands were found high.[22,24]

The natural basis set for a periodic crystal is a Fourier series of plane waves.[29] Program CASTEP employs density functional theory[30] with a generalized gradient approximation[15] for the exchange-correlation energy and a plane-wave basis set to build the wave functions. The explicit treatment of valence electrons combined with pseudopotentials[15] for the nuclei and core electrons has been shown to be effective in the study of proton-transfer catalysis within aluminosilicate zeolite pores.[31,32] The program approximates the calculation for an infinite crystal by repeating the central unit cell (here, 41−42 atoms) along the three crystal axes. It is an important aspect of this approach that the long-range electrostatic environment in periodic systems

10.1021/jp0132127 CCC: $22.00
Published on Web 05/09/2002

TABLE 1: Ab Initio Structure of Pyrophyllite Compared with the Crystal Structure

mineral parameter	CASTEP[a]	experiment[b]
a axis length	5.136	5.160
b axis length	8.957	8.966
c axis length	9.511	9.347
α cell angle	90.70	91.18
β cell angle	100.09	100.46
γ cell angle	89.61	89.64
layer d spacing[c]	9.363	9.190
density (g cm^{-3})	2.778	2.815
Al−O bond length	1.899 ± 0.023	1.912 ± 0.017
Si−O bond length	1.597 ± 0.010	1.617 ± 0.011
O−H bond length	0.959	0.971

[a] The program CASTEP was used[15] with the 330 eV basis set and GGA theory. Distances are in angstroms, and angles are in degrees. [b] Crystallographic data from Lee and Guggenheim.[43] [c] Defined as the crystallographic repeat distance normal to the *ab* plane.

reveals phenomena, which ab initio calculations of isolated clusters of similar systems will not produce.

From the oxidized nontronite system defined above, a reduced model nontronite structure was constructed by adding to the unit cell one more electron and one more Na^+ to balance its charge. A comparison of structures for oxidized[6,16] and reduced[5] nontronites yields a consistent model[33] for the stoichiometry of the reduction process.

In the reduced nontronite system obtained as described above, for simplicity, all Fe atoms were left in cis sites. This is a highly idealized structure and different from naturally occurring reduced nontronites,[6] but we accepted it a suitable model for the exploratory calculations described in this paper. Other systems, including larger ones if possible, will be considered in the future. For the current reduced nontronite, the optimization process was repeated, and a fully optimized structure was obtained.

All geometry optimizations performed for this study included the atomic positions of the adsorbates and nontronite within the experimental unit cell, in addition to the unit cell lengths and angles, achieving full optimization of the entire crystal system. The default convergence criteria of CASTEP were applied; that is, 0.0002 eV for the energy change per atom, 0.001 Å for the rms atomic displacement, and 0.05 eV/Å for the rms residual force. The 330 eV basis set was used with the gradient corrected local spin density approximation[15] and 19 free spins for reduced nontronite, assuming high-spin states for all Fe. The versions of CASTEP included in the Cerius[2] software package were used, issues 3.8 and 4.0, obtained from MSI Corp.[34]

To study the structure of TCE on nontronite, the layers of the reduced structure of nontronite, $Na_2(AlSi_7)Fe_4O_{20}(OH)_4$, were arbitrarily separated to 15 Å, a single molecule of TCE was introduced, and the entire system was optimized. In a second case, one molecule of TCE was introduced into the interlayer space of reduced nontronite together with eight water molecules. After geometry optimization of this system, it was subjected to ab initio molecular dynamics (MD) simulations. The default criteria of Cerius[2] for MD simulations[34] were applied, total spin 19, external temperature 298 K, kinetic energy cutoff 330 eV, time step 0.5 fs, and the NVT dynamic ensemble. All calculations were performed on an IBM RS/6000 model 260 workstation.

Results and Discussion

Some structural results from the calculations are presented in Tables 1−4. Views of TCE in the nontronite interlayer space, with water present and without, are presented in Figures 1 and 2. Results from the quantum dynamics simulations are presented in Figures 3−9.

TABLE 2: Ab Initio Structure of Talc Compared with the Crystal Structure

mineral parameter	CASTEP[a]	experiment[b]
a axis length	5.293	5.291
b axis length	5.299	5.290
c axis length	9.607	9.460
α cell angle	98.76	98.68
β cell angle	85.15	85.27
γ cell angle	120.02	119.90
layer d spacing[c]	9.494	9.351
density (g cm^{-3})	2.731	2.776
Mg−O bond length	2.095 ± 0.020	2.072 ± 0.018
Si−O bond length	1.610 ± 0.007	1.622 ± 0.002
O−H bond length	0.961	0.846

[a] The program CASTEP was used[15] with the 330 eV basis set and GGA theory. Distances are in angstroms, and angles are in degrees. [b] Crystall structure by Perdikatsis and Burzlaff.[44] The talc H-atom positions were estimated. [c] Defined as the crystallographic repeat distance normal to the *ab* plane.

TABLE 3: Ab Initio Structure of Kaolinite Compared with the Crystal Structure

mineral parameter	CASTEP[a]	experiment[b]
a axis length	5.150	5.154
b axis length	8.942	8.942
c axis length	7.492	7.391
α cell angle	91.52	91.93
β cell angle	104.70	105.05
γ cell angle	89.88	89.80
layer d spacing[c]	7.244	7.131
density (g cm^{-3})	2.570	2.608
Al−O bond length	1.895 ± 0.073	1.908 ± 0.019
Si−O bond length	1.600 ± 0.010	1.615 ± 0.004
O−H bond length	0.961 ± 0.002	0.978 ± 0.004

[a] The program CASTEP was used[15] with the 330 eV basis set and GGA theory. Distances are in angstroms, and angles are in degrees. [b] Crystal structure by Bish.[45] [c] Defined as the crystallographic repeat distance normal to the *ab* plane. This value is reported in lieu of the *c* axis length because relative translations of adjacent lamellae during molecular dynamics will often result in distorted values for *c*, even though the d spacing remains essentially constant.

(a) Some General Structural Trends. To gain some experience with the performance of CASTEP in modeling the structures of clay minerals, geometry optimizations were performed for some benchmark systems. Results obtained for pyrophyllite, talc, and kaolinite are presented in Tables 1−3 and compared with the crystal structures. The largest deviations between calculated and experimental structures (∼0.1−0.2 Å) are found for the relatively long (∼9 Å) *c* axis and d_{001} spacing, whereas bond lengths within the crystal lattice agree within ∼0.02 Å. Calculated d_{001} spacings are typically longer than experimental values (Tables 1−3) which is in agreement with the fact that long-range dispersion forces are absent in the density functional calculations.

The model oxidized nontronite that we created, of unit cell formula $Na(AlSi_7)Fe_4O_{20}(OH)_4$, is an idealized ferric end-member for the nontronites, yet it is quite close in composition to the well-studied Garfield nontronite, which has the formula $Na_{1.07}(Al_{0.98}Si_{7.02})(Fe_{3.72}Al_{0.23}Mg_{0.03})O_{20}(OH)_4$.[35] There is some uncertainty in this formula, with various studies reporting 0.78−1.16 tetrahedral charges per unit cell.[6,16,36−40] The layer charge is almost completely due to tetrahedral Al. A detailed crystal structure refinement[16] is available. It is compared with the CASTEP computational results in Table 4. Again, the differences between computed and experimental structures are largest

TABLE 4: Ab Initio Structures (Distances in Angstroms, Angles in Degrees) of Oxidized and Reduced Nontronite Compared with Crystal Structure Refinements

mineral parameter	oxidized CASTEP model[a]	oxidized expt[b]	reduced CASTEP model[c]	reduced expt[d]	with TCE, H_2O in interlayer[e]
a axis length	5.279	5.277	5.279	5.21	5.255
b axis length	9.114	9.140	9.158	9.21	9.132
c axis length	10.056	9.780	10.057	∼9.91	20.287
α cell angle	90.57	90.00	88.76	∼90	89.27
β cell angle	100.58	101.00	99.81	∼101	100.33
γ cell angle	90.03	90.00	89.95	∼90	90.00
layer d spacing[f]	9.885	9.600	9.908	9.732	19.957
density (g cm^{-3})	2.996	3.077	3.054	∼3.13	2.005
Fe−O bond length	2.014 ± 0.030	2.013 ± 0.032	2.045 ± 0.044	2.10	2.014 ± 0.029
Si−O bond length	1.606 ± 0.011	1.645 ± 0.013[b]	1.612 ± 0.020		1.605 ± 0.013
Al−O bond length	1.711 ± 0.017	*b*	1.722 ± 0.012		1.706 ± 0.017
O−H bond length	0.968 ± 0.003	1.000[b]	0.968 ± 0.001		0.970 ± 0.004
Na···O distances	3.166 ± 0.511	3.031 ± 0.199	3.162 ± 0.356		

[a] Program CASTEP was used[15] with the 330 eV basis set and GGS theory with 20 unpaired spins. [b] Manceau et al.[6] Hydrogen positions were not solved in the experimental structure, so they were added for the present study. The refined tetrahedral bond lengths are weighted averages of Si−O and Al−O. The experimental *c* axis length was adjusted to 9.78 Å and is not an experimental observable. For this reason, the precision on Na-to-basal-oxygen distances is low for the experimental structure. [c] Program CASTEP,[15] 330 eV basis set, GGS theory, 19 unpaired spins. [d] Manceau et al.[5] Only *a*, *b*, d_{001}, and the Fe−O distance were reported. [e] Program CASTEP,[15] 330 eV basis set, GGS theory, 19 unpaired spins. [f] Defined as the crystallographic repeat distance normal to the *ab* plane.

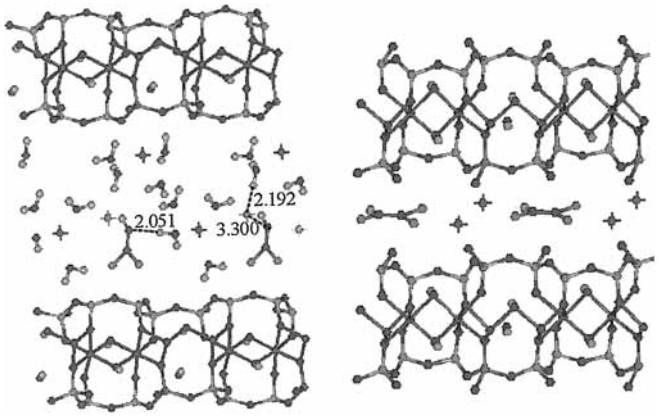

Figure 1. Optimized structure of nontronite with trichloroethene in the interlayer space; in the presence of water (left) and without water (right). In the dry system (right), TCE is adsorbed flat and without change on the mineral basal plane. When the same system is optimized with water in the interlayer space (left), geometry optimization leads to a structure in which Cl has dissociated from TCE. The Cl atom is at a distance of 3.3 Å to the C atom from which it dissociated and forms an H bond to a water molecule at 2.19 Å. The dissociated C atom also forms an H bond with water, at 2.05 Å.

for the *c* axis and d_{001} spacing. The average Fe−O bond length in the modeled structure of the oxidized nontronite agrees well with the observed value of 2.01 Å,[6] with a range of 1.95−2.08 Å.

The CASTEP minimum-energy geometry for the reduced nontronite has a longer *b* axis and longer Fe−O bonds than the oxidized model (Table 4). Experimentally,[5,6] full reduction (i.e., four electrons per unit cell) of the Garfield nontronite results in an expansion of the *b* axis from 9.14 to 9.21 Å. In the present calculations, only a single electron was added to the four-Fe unit cell. Accordingly, the computed increase in the *b* axis is smaller, i.e., 0.044 Å (Table 4). In contrast to the experimental results, the computed *a* axis did not shrink upon reduction of the structural Fe. The average computed Fe−O bond length for the singly reduced nontronite is 0.03 Å larger than in the oxidized form, which should be compared to an increase of ∼0.09 Å for the quadruply reduced experimental crystal. In addition, the standard deviation of the computed bond lengths increases upon reduction, in agreement with experimental observations that Fe−O distances become more structured upon reduction.[5] Experimental estimates for Fe(II)−O in fully reduced clays show a characteristic bond length of 2.10 Å.[5] Interestingly, in the current study, the average of the six longest Fe−O bonds (of the 24 unique Fe−O bonds) is indeed 2.103 Å.

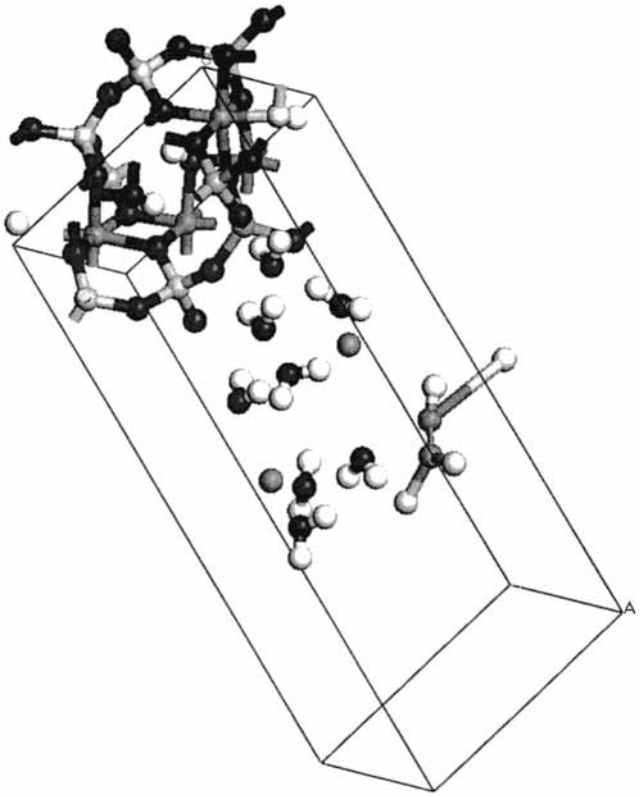

Figure 2. Enlarged view of the optimized structure of nontronite with trichloroethene and eight water molecules in the interlayer space. Note the nonplanarity of trichloroethene and the visibly elongated C*−Cl* distance at the H−C−Cl end of the molecule.

In both nontronite models, the CASTEP calculations indicate that the unhydrated Na^+ ions do not reside at the midplane of the interlayer space. In the oxidized model, the Na^+ is shifted 0.41 Å toward the side of the interlayer in which Al has substituted for Si in a tetrahedral site. In the reduced model, the two Na^+ are shifted 0.57 ± 0.01 Å toward the same side.

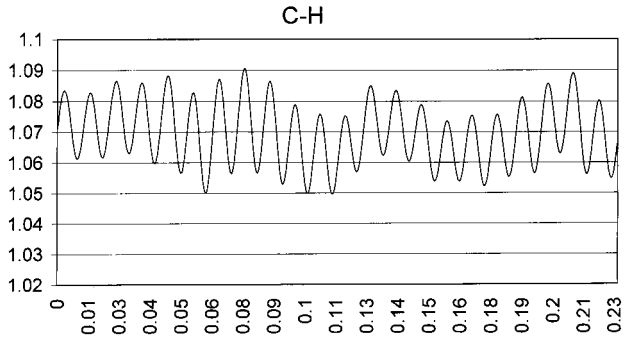

Figure 3. Evolution of the C−H bond distance in trichloroethene on nontronite with water, during molecular dynamics. The absicissa is the time axis and scaled in picoseconds. The ordinate is the distance axis and scaled in angstroms.

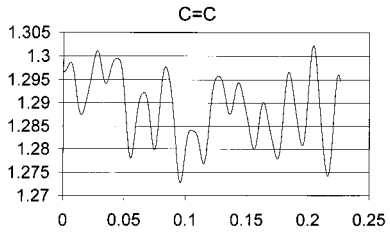

Figure 4. Evolution of the C═C bond distance in trichloroethene on nontronite with water, during molecular dynamics. The abscissa is the time axis and scaled in picoseconds. The ordinate is the distance axis and scaled in angstroms.

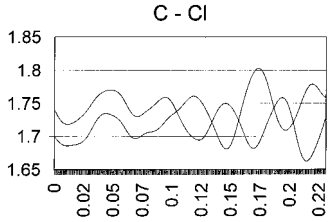

Figure 5. Evolution of the two C−Cl bond distances at the Cl−C−Cl end of trichloroethene on nontronite with water, during molecular dynamics. The abscissa is the time axis and scaled in picoseconds. The ordinate is the distance axis and scaled in angstroms.

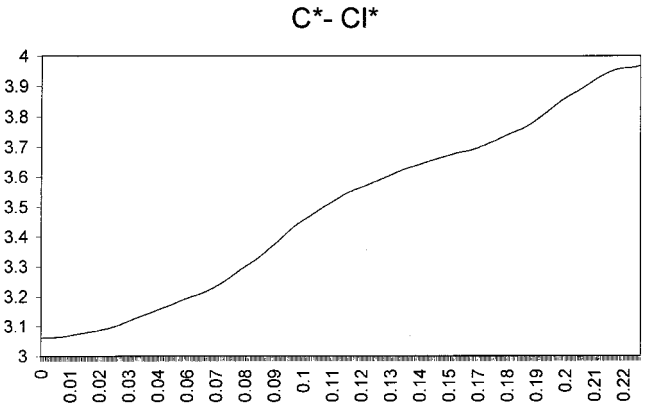

Figure 6. Evolution of the C*−Cl* distance at the H−C−Cl end of trichloroethene on nontronite with water, during molecular dynamics. The abscissa is the time axis and scaled in picoseconds. The ordinate is the distance axis and scaled in angstroms.

A structural difference between the oxidized and reduced forms of notronite is of specific interest for the discussion below. It concerns the optimized angles formed by the four unique structural O−H bonds with the octahedral plane. They are 21°, 4°, 2°, and 1°, in the minimum-energy structure of the oxidized

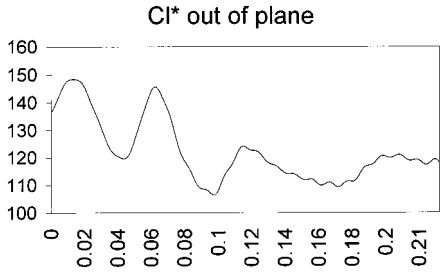

Figure 7. Evolution of the Cl*-out-of-plane angle at the H−C−Cl end of trichloroethene on nontronite with water, during molecular dynamics. The abscissa is the time axis and scaled in picoseconds. The ordinate is the angle axis and scaled in degrees.

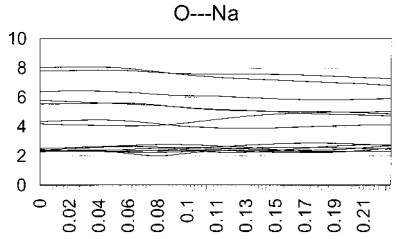

Figure 8. Evolution of the O···Na nonbonded distances in the trichloroethene/nontronite/water system, during molecular dynamics. The abscissa is the time axis and scaled in picoseconds. The ordinate is the distance axis and scaled in angstroms.

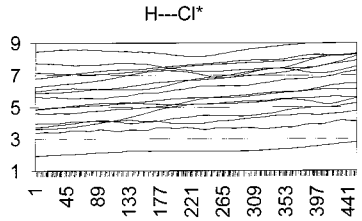

Figure 9. Evolution of the $(H_2O)H\cdots Cl^*$ nonbonded distances in the trichloroethene/nontronite/water system, during molecular dynamics. The abscissa is the time axis and scaled by step number. The ordinate is the distance axis and scaled in angstroms.

nontronite, with the two largest angles belonging to the hydroxyls closest to the Al substitution site. In the CASTEP minimum-energy geometry for the reduced nontronite, the O−H vectors are essentially parallel to the octahedral plane with angles of 1°, 6°, 1°, and 2° (same ordering as for the oxidized nontronite), so they have relaxed by up to 20° compared to the oxidized nontronite.

(b) Some Selected Structural Aspects of Trichloroethene in the Nontronite Interlayer Space. When the TCE/nontronite system is optimized in the absence of water, a structure results in which the molecule resides flat on the mineral basal plane (Figure 1). That kind of interaction is characteristic for the adsorption of organic compounds on clay mineral surfaces. It has been found before[41] in empirical molecular dynamics simulations of TCE on pyrophyllite and kaolinte, and it has been observed for the adsorption of methylene blue[42] on mineral surfaces, and the same configuration is being obtained in ongoing studies in our group of the interactions of various pesticides with clay minerals.

In the absence of water (Figure 1), the molecular structure of adsorbed TCE is not distinguished by any unusual features, compared to free TCE. Bond distances and angles are in the expected ranges: the C−Cl bond lengths, specifically, are ∼1.70 Å, and the molecule is essentially planar; the *cis*-Cl−C═C−Cl torsion is 1.3°. In contrast (Figure 2), when the geometry of the TCE/nontronite system is optimized in the presence of water

in the interlayer space, the *cis*-Cl−C═C−Cl torsion changes to 52.5°, and the C−Cl bond at the H−C−Cl end of TCE (henceforth referred to as C*-Cl*) seems to have been broken, because it has increased to ∼3 Å. The participation of water for this result seems essential, considering that the C*−Cl* bond elongation is not found for the dry system (Figure 1) and the fact that there are close nonbonded H···Cl* and H···C* interactions with water at 2.19 and 2.05 Å, respectively (Figure 1).

There is a variety of circumstantial evidence indicating that the clay, which began the simulation with the reduced structure, has become oxidized by the addition of TCE with water and the subsequent geometry optimization of the entire system: The resulting structure of the clay is closer to the oxidized structure than the one reduced (Table 4). First, the mean Fe−O bond length is 2.01 Å, which is characteristic of the oxidized structure, and there is no Fe−O bond longer than 2.05 Å. Also, the Si−O and Al−O bond lengths are shorter than their counterparts in the reduced model, more nearly matching those in the oxidized model. Finally, the structural O−H vectors relaxed from their essentially parallel arrangement with respect to the octahedral plane in the starting structure, back to angles of 26°, 5°, 3°, and 1°, which is characteristic for the oxidized clay structure rather than the reduced as shown above.

(c) Some Selected Results of the Molecular Dynamics Simulations. The idealized nature of our system has been emphasized above. For that system, nevertheless, the structural changes are clear. It is possible that the starting geometry of TCE on nontronite, with the placement of surrounding water, was fortuitously high in energy, so that the system was able to overcome the barrier to C−Cl dissociation, which can in principle be small for TCE in the interlayer space. Nevertheless, to make sure that the optimized system was not a false energy minimum, the optimized TCE/water/nontronite system was subjected to additional molecular dynamics simulations. Because of the length of the calculations, the dynamics simulations were restricted to some 400 steps, or ∼0.2 ps. As it turns out, the results are sufficient to support the conclusions of this study.

The evolution of interatomic distances in the TCE/water/nontronite system during molecular dynamics is documented in Figures 3−9. The figures show the oscillations characteristic for bonded distances, with frequencies of ∼3240 cm^{-1} for H−C (Figure 3), ∼1680 cm^{-1} for C═C (Figure 4), and ∼780 and ∼690 cm^{-1} for the two C−Cl bonds (Figure 5) at the Cl−C−Cl end of TCE. In addition, the distance evolution is shown for C*−Cl* (Figure 6), the Cl* out-of-plane motion (Figure 7), and various low-frequency oscillations are seen for the shallow potential energy curves of nonbonded distances, such as O···Na and H−Cl* (Figures 8 and 9). High-frequency oscillations such as those of H−C and C═C are enveloped with the effects of low-frequency oscillations. Thus, the oscillatory motion displayed in Figures 3−9 are not normal modes but the sum total of the effects of all the normal modes of the system on a given internuclear distance.

Comparison of the two C−Cl and the C*−Cl* oscillations (Figures 5 and 6) show characteristic differences. Although the former display the periodic behavior typical for bonds, the C*−Cl* distance increases steadily from ∼ 3 to 4 Å over the period of investigation, showing nothing but the soft oscillations of a shallow potential. It is also interesting to note that, initially, the Cl* out of plane motion followed a definite oscillatory pattern (Figure 7) until, at ∼0.1 ps, a transition occurs to a different kind of motion. At about the same time, the two C−Cl bonds at the Cl−C−Cl end of TCE go out of phase, after initially moving in phase for ∼0.1 ps. Thus, trajectories of this kind provide an interesting illustration on internal vibrational interactions.

It is also interesting to consider the nonbonded interactions, such as O···Na and H···Cl*. They show that the entire cell is a network of shallow potential energy interactions and concomitant low-frequency oscillations.

Conclusions

From the material presented above, the idealized nature of the TCE/water/nontronite model system investigated here is obvious. Similarly, the idealized nature of the calculations is apparent from the many simplifying assumptions adopted for them. Nevertheless, even for an idealized system, the results are highly unusual. At the same time, the internal consistency of the calculated structural trends and the generally good agreement between X-ray crystallographic structures and calculated geometries (see Tables 1−4) convey the impression that our model system is not unrealistic.

It is well-known[46] that, under certain conditions, density functional theory may incorrectly predict no barrier for low-barrier chemical reactions. In the current case, this imperfection revealed what seems to be a characteristic aspect of the decomposition of TCE on nontronites; that is, the reductive dechlorination of TCE occurs more readily when water is present than when it is not. Thus, apart from TCE and its potential fate on nontronite, the results of this study make it interesting to investigate to what extent computational techniques can be used in cooperation with laboratory techniques in helping to optimize the experimental conditions under which particular catalytic reactions are most likely to proceed.

Acknowledgment. The authors gratefully acknowledge support by USDA CSREES Grant 99-35107-7782 and by the IBM Shared University Research Program. Special thanks are due to Prof. Collis Geren, Vice Chancellor for Research, University of Arkansas, and Dr. Jamie Coffin, IBM. L.S. thanks Professor J. W. Stucki for his helpful review of the manuscript.

References and Notes

(1) Stucki, J. W.; Roth, C. B. *Soil Sci. Soc. Am. J.* **1977**, *41*, 808−814.
(2) Komadel, P.; Lear, P. R.; Stucki, J. W. *Clays Clay Miner.* **1990**, *38*, 203−208.
(3) Komadel, P.; Madejova, J.; Stucki, J. W. *Clays Clay Miner.* **1995**, *43*, 105−110.
(4) Stucki, J. W.; Bailey, G. W.; Gan, H. M. *Appl. Clay Sci.* **1996**, *10*, 417−430.
(5) Manceau, A.; Drits, V. A.; Lanson, B.; Chateigner, D.; Wu, J.; Huo, D.; Gates, W. P.; Stucki, J. W. *Am. Mineral.* **2000**, *85*, 153−172.
(6) Manceau, A.; Lanson, B.; Drits, V. A.; Chateigner, D.; Gates, W. P.; Wu, J.; Huo, D.; Stucki, J. W. *Am. Mineral.* **2000**, *85*, 133−152.
(7) Hofstetter, T. B.; Heijman, C. G.; Haderlein, S. B.; Holliger, C.; Schwarzenbach, R. P. *Environ. Sci. Technol.* **1999**, *33*, 1479−1487.
(8) Schwarzenbach, R. P.; Angst, W.; Holliger, C.; Hug, S. J.; Klausen, J. *Chimia* **1997**, *51*, 908−914.
(9) Pecher, K.; Haderlein, S. B.; Schwarzenbach, R. P. *Abstr. Papers Am. Chem. Soc.* **1997**, *213*, 189-ENVR.
(10) Fruchter, J. S.; Cole, C. R.; Williams, M. D.; Vermeul, V. R.; Amonette, J. E.; Szecsody, J. E.; Istok, J. D.; Humphrey, M. D. *Ground Water Monit. Rem.* **2000**, *20*, 66−77.
(11) Istok, J. D.; Amonette, J. E.; Cole, C. R.; Fruchter, J. S.; Humphrey, M. D.; Szecsody, J. E.; Teel, S. S.; Vermeul, V. R.; Williams, M. D.; Yabusaki, S. B. *Ground Water* **1999**, *37*, 884−889.
(12) Nzengung, V. A.; Mills, G. L.; Heath, B. *Abstr. Papers Am. Chem. Soc.* **1999**, *217*, 078-GEOC.
(13) Cervini-Silva, A.; Wu, J.; Larson, R. A.; Stucki, J. W. *Environ. Sci. Technol.* **2000**, *34*, 915−917.
(14) Cervini-Silva, J.; Wu, J.; Stucki, J. W.; Larson, R. A. *Clays Clay Miner.* **2000**, *48*, 132−138.

(15) Payne, M. C.; Teter, M. P.; Allan, D. C.; Arias, T. A.; Joannopoulos, J. D. *Rev. Modern Phys.* **1992**, *64*, 1045−1097.
(16) Manceau, A.; Chateigner, D.; Gates, W. P. *Phys. Chem. Miner.* **1998**, *25*, 347−365.
(17) Hoffmann, R. *Solids and surfaces: A chemist's view of bonding in extended structures*; VCH Publishers: New York, 1988.
(18) Bleam, W. F. *Clays Clay Miner.* **1990**, *38*, 522−526.
(19) Bleam, W. F. *Clays Clay Miner.* **1990**, *38*, 527−536.
(20) Bleam, W. F.; Hoffmann, R. *Phys. Chem. Miner.* **1988**, *15*, 398−408.
(21) Dovesi, R.; Roetti, C.; Freyria-Fava, C.; Aprà, E.; Saunders: V. R.; Harrison, N. M. *Philos. Trans. R. Soc. London, Ser. A* **1992**, *341*, 203-210.
(22) Pisani, C. *J. Mol. Struct. (THEOCHEM)* **1999**, *463*, 125−137.
(23) Pisani, C.; Dovesi, R.; Roetti, C. *Hartree−Fock ab initio treatment of crystalline systems*; Springer-Verlag: Berlin, 1988.
(24) Hess, A. C.; Saunders: V. R. *J. Phys. Chem.* **1992**, *96*, 4367−4374.
(25) Nicholas, J. B.; Hess, A. C. *J. Am. Chem. Soc.* **1994**, *116*, 5428−5436.
(26) Stave, M. S.; Nicholas, J. B. *J. Phys. Chem.* **1995**, *99*, 15046−15061.
(27) White, J. C.; Hess, A. C. *J. Phys. Chem.* **1993**, *97*, 8703−8706.
(28) White, J. C.; Hess, A. C. *J. Phys. Chem.* **1993**, *97*, 6398−6404.
(29) Bloch, F. *Z. Phys.* **1928**, *52*, 555−600.
(30) Kohn, W.; Becke, A. D.; Parr, R. G. *J. Phys. Chem.* **1996**, *100*, 12974−12980.
(31) Shah, R.; Payne, M. C.; Lee, M.-H.; Gale, J. D. *Science* **1996**, *271*, 1395−1397.
(32) Shah, R.; Gale, J. D.; Payne, M. C. *J. Phys. Chem.* **1996**, *100*, 11688−11697.
(33) Drits, V. A.; Manceau, A. *Clays Clay Miner.* **2000**, *48*, 185−195.
(34) *MSI.*; Molecular Simulations, Inc.; currently Accelrys Inc.: San Diego, CA, 1999.
(35) Gates, W. P. Personal communication, 2000.
(36) Senkayi, A. L.; Dixon, J. B.; Hossner, L. R.; Kippenberger, L. A. *Soil Sci. Soc. Am. J.* **1985**, *49*, 1054−1060.
(37) Lear, P. R.; Stucki, J. W. *Clays Clay Miner.* **1987**, *35*, 373−378.
(38) Sherman, D. M.; Vergo, N. *Am. Mineral.* **1988**, *73*, 1346−1354.
(39) Luca, V. *Clays Clay Miner.* **1991**, *39*, 467−477.
(40) Luca, V.; Maclachlan, D. J. *Clays Clay Miner.* **1992**, *40*, 1−7.
(41) Teppen, B. J.; Yu, C.-H.; Miller, D. M.; Schäfer, L. *J. Comput. Chem.* **1998**, *19*, 144−153.
(42) Yu, C.-H.; Newton, S. Q.; Norman, M. A.; Miller, D. M.; Schäfer, L.; Teppen, B. J. *Clays Clay Miner.* **2000**, *48*, 665−681.
(43) Lee, J. H.; Guggenheim, S. *Am. Mineral.* **1981**, *66*, 350−357.
(44) Perdikatsis, B.; Burzlaff, H. *Z. Kristallogr.* **1981**, *156*, 177−186.
(45) Bish, D. L. *Clays Clay Miner.* **1993**, *41*, 738−744.
(46) Baker, J.; Andzelm, J.; Muir, M.; Taylor, P. R. *Chem. Phys. Lett.* **1995**, *237*, 53−60.